Inorg. Chem. **2009**, *48*, 541−548

Quantum Chemical Studies on High-Valent Metal Nitrido Derivatives of Keggin-Type Polyoxometalates ($[PW_{11}O_{39}\{M^{VI}N\}]^{4-}$ (M = Ru, Os, Re)): M^{VI}−N Bonding and Electronic Structures

Chun-Guang Liu, Zhong-Min Su,* Wei Guan, and Li-Kai Yan

Institute of Functional Material Chemistry, Faculty of Chemistry, Northeast Normal University, Changchun 130024, P. R. China

Received July 3, 2008

High-valent M^{VI}≡N (M = Ru, Os) species are important reagents in nitrogen transfer reactions; the unique withdrawing properties of polyoxometalate (POMs) ligands would possibly modify the reactivity of the M^{VI}≡N functional group. In the present paper, density functional theory (DFT) and natural bond orbital (NBO) analysis have been employed to calculate electronic structures, M^{VI}−N bonding, and redox properties of high-valent metal nitrido derivatives of Keggin-type POMs, $[PW_{11}O_{39}\{M^{VI}N\}]^{4-}$ (M = Ru, Os, Re). Our calculations show that $[PW_{11}O_{39}\{RuN\}]^{4-}$ possesses stronger antibonding interaction between metal and nitrogen atoms compared with anions $[PW_{11}O_{39}\{OsN\}]^{4-}$ and $[PW_{11}O_{39}\{ReN\}]^{4-}$. A large increase in the Ru−N bond length of anion $[PW_{11}O_{39}\{RuN\}]^{4-}$ in the excited states has been found; the effective order and composition of the molecular orbital in anion $[PW_{11}O_{39}\{RuN\}]^{4-}$ is a key factor in determination of the increase of the Ru−N bond length in the excited states. The substitution effects of central tetrahedron heteroatoms (XO_4, X = Al, Si, P, As) in anions $[XW_{11}O_{39}\{RuN\}]^{4-}$ affect the relative energy of the LUMO; the relevant orbital energy increases in the order Al(III) < Si(IV) < P(V) ≈ As(V). The RuN unit is the reduced center. NBO analysis of the extent of the bonding interaction between the ruthenium and the nitrogen centers in $[PW_{11}O_{39}\{Ru^{VI}N\}]^{4-}$ shows that the Ru−N bond possesses a covalent feature and displays triple-, double-, and single-bond character when moving along the change of spin state (^{1}**1** → ^{3}**1** → ^{5}**1**).

1. Introduction

Utilization of metal nitrido compounds (LM≡N) as an N-atom source in synthesis is receiving increasing attention because of their potential role in aziridination, nitrogen fixation, and other processes.[1] Nitrido complexes of manganese(V) porphyrin,[2] manganese(V) salen,[3] and ruthenium(VI) porphyrin[4] have been used as reagents for the aziridination of alkenes; however, these complexes need to be activated with an electrophile such as trifluoroacetic anhydride to produce imido complexes as the active species. Various approaches including replacement of the metal in the nitridometal (M≡N) functional group (such as M = Mn, Fe, Ru, Os, Re, etc.) and modification of the electronic properties of the M≡N functional group by introduction of new ancillary ligands (L) (such as L = porphyrin, Schiff base, aniline, terpyridyl, etc.) have been employed to activate the M≡N functional group. Among them, the high-valent ruthenium(VI) porphyrin species constitute an important family because of the extraordinary versatility in binding N-donating ligands at the axial sites.[5] For the ancillary ligand, it is an interesting functionality, the reactivity of which is sensitive to the ancillary ligands on the metal center. The M≡N functional group can display electrophilic or nucleophilic by modifying ancillary ligands.[6] Compounds with

* To whom correspondence should be addressed. E-mail: zmsu@nenu.edu.cn.

(1) (a) Bois, J. D.; Tomooka, C. S.; Hong, J.; Carreira, E. M. *Acc. Chem. Res.* **1997**, *30*, 364. (b) Eikey, R. A.; Abu-Omar, M. M. *Coord. Chem. Res.* **2003**, *243*, 83.

(2) Groves, J. T.; Takahashi, T. *J. Am. Chem. Soc.* **1983**, *105*, 2073.

(3) (a) Minakata, S.; Ando, T.; Nishimura, M.; Ryu, L.; Komatsu, M. *Angew. Chem., Int. Ed.* **1998**, *37*, 3392. (b) Fang, G. S.; Huang, J. S.; Zhu, N.; Che, C. M. *Eur. J. Inorg. Chem.* **2004**, *43*, 1341. (c) Man, W. L.; Lam, W. W. Y.; Yiu, S. M.; Lau, T. C.; Peng, S. M. *J. Am. Chem. Soc.* **2004**, *126*, 15336.

(4) (a) Huang, J. S.; Che, C. M.; Poon, C. K. *J. Chem. Soc., Chem. Commun.* **1992**, 161. (b) Au, S. M.; Huang, J. S.; Yu, W. Y.; Fung, W. H.; Che, C. M. *J. Am. Chem. Soc.* **1999**, *121*, 9120. (c) Zhou, X. G.; Yu, X. Q.; Huang, J. S.; Che, C. M. *Chem. Commun.* **1999**, 2377. (d) Sun, X. R.; Huang, J. S.; Cheung, K. K.; Che, C. M. *Inorg. Chem.* **2000**, *39*, 820. (e) Yi, G. B.; Khan, M. A.; Powell, D. R.; Richter-Addo, G. B. *Inorg. Chem.* **1998**, *37*, 208. (f) Lee, J.; Yi, G. B.; Khan, M. A.; Richter-Addo, G. B. *Inorg. Chem.* **1999**, *38*, 4578.

10.1021/ic8012443 CCC: $40.75
Published on Web 12/12/2008

electrophilic multiply bonded ligands are good candidates to be oxidants because they can potentially add nucleophiles directly at the ligand. For example, the osmium nitridos undergo direct a [4 + 1] cycloaddition reaction with electron-rich cyclohexadienes to produce bicyclic osmium amido complexes in which the nitrogen atom inserts between the two carbons of the alkene.[7]

For about two decades, the transition-metal-substituted Keggin-type polyoxometalates (POMs) have been found to have catalytic properties in oxygen transfer reactions;[8] moreover, these catalysts sometimes exhibit features that are superficially similar to those observed with analogous metalloporphyrins. Thus, the lacunary ligand, $[PW_{11}O_{39}]^{7-}$ in Keggin-type POMs, can be viewed as a porphyrin-like ligand. It has been suggested that this ligand can act as a potential multielectron acceptor[9] and has been adopted to activate the metal oxygen compounds with an oxygen donor. Analogously, the unique withdrawing properties of POM ligands would possibly modify the reactivity of the M≡N functional group.

Proust and co-worker synthesized and structurally characterized a series of high-valent metal nitrido derivatives of Keggin typical POMs, especially the hexavalent species, $(n\text{-}Bu_4N)_4[PW_{11}O_{39}(M^{VI}N)]$ (M = Ru, Os, Re);[10] moreover, the reactivity of these nitrido derivatives of POMs toward nucleophilic or electrophilic reagents and nitrogen-atom transfer to olefins have been considered. Among them, the electrophilic reactivity of phosphotungsto−ruthenate heteropolyanion, $[PW_{11}O_{39}\{RuN\}]^{4-}$,[10c] has been verified successfully. The results showed that $[PW_{11}O_{39}\{Ru^{VI}N\}]^{4-}$ can react with triphenylphosphine and released the bis(triphenylphosphane)iminium cation $[PPh_3{=}N{=}PPh_3]^+$ through several intermediates. This is combined with examples of alkene amination and aziridination by ruthenium−nitrido porphyrin and ruthenium−nitrido salen complexes, which proved the versatility of the reactivity of the ruthenium−nitrido functional group corresponding to the diverse ancillary ligands.[4] However, comparing it with the ruthenium−nitrido functional group in the lacunary ligand $[PW_{11}O_{39}]^{7-}$, $[PW_{11}O_{39}(Re^{VI}N)]^{4-}$, gave disappointing reactivity.[10c] These differences in reactivity for high-valent metal nitrido derivatives of Keggin typical POMs let us undertake a computational examination of this area.

Quantum chemistry calculations based on the density functional theory (DFT) formalism is a useful tool for understanding and rationalizing the electronic structure and reactivity of high-valent metal derivatives of Keggin-type POMs anions and analogous high-valent metal complexes. Such as, systematic DFT studies of the POM−Fe=O^{4-} and the oxidized form, POM−Fe=O^{3-},[11] DFT and natural bond orbital (NBO) studies of electronic structures, spectroscopy of mononuclear, nonheme$\{Fe-NO\}^6$ complexes,[12] and magnetic circular dichroism spectroscopy combining with DFT studies of the excited-state structures and bonding in nonheme Fe^{IV}=O complexes,[13] etc. these results were very useful in the analysis of its catalytic properties and reactivity. In the present paper, we report a detailed DFT and NBO study on the anions $[PW_{11}O_{39}\{MN\}]^{4-}$ (**1**, M = Ru; **2**, M = Os; **3**, M = Re) and analyze their electronic structures and chemical bonding features between the M and N atoms in these POMs anions.

2. Computational Methodology

All of anions studied here were optimized with the BP86[14] generalized gradient approximations, VWN local density functional,[15] triple-ζ basis plus polarization Slater-type orbital basis sets, and the integration parameter 6.0 as implemented in the ADF 2006 program system.[16] The 1s shell of N and O, 1s to 2p shells for Al, Si, and P, 1s to 3d shells for As and Ru, and 1s to 4d shells for W, Os, and Re have been treated by the frozen core approximation. The relativistic effects were taken into account using the zeroth order regular approximation (ZORA).[17] The continuum solvation model COSMO[18] and a dielectric constant of acetonitrile have been performed for solvent effects in this work. The van der Waals radii for the POM atoms, which actually define the cavity in the COSMO,

(5) (a) Antipas, A.; Buchler, J. W.; Gouterman, M.; Smith, P. D. *J. Am. Chem. Soc.* **1978**, *100*, 3015. (b) Richter-Addo, G. B.; Wheeler, R. A.; Hixson, C. A.; Chen, L.; Khan, M. A.; Ellison, M. K.; Schulz, C. E.; Scheidt, W. R. *J. Am. Chem. Soc.* **2001**, *123*, 6314. (c) Groves, J. T.; Ahn, K. H.; Qunn, R. *J. Am. Chem. Soc.* **1988**, *110*, 4217.

(6) (a) Marshman, R. W.; Shapley, P. A. *J. Am. Chem. Soc.* **1990**, *112*, 8369. (b) Crevier, T. J.; Bennett, B. K.; Soper, J. D.; Bowman, J. A.; Dehestani, A.; Hrovat, D. A.; Lovell, S.; Kaminsky, W.; Mayer, J. M. *J. Am. Chem. Soc.* **2001**, *123*, 1059.

(7) Maestri, A. G.; Cherry, K. S.; Toboni, J. J.; Brown, S. N. *J. Am. Chem. Soc.* **2001**, *123*, 7459.

(8) (a) Kumar, D.; Derat, E.; Khenkin, A. M.; Neumann, R.; Shaik, S. *J. Am. Chem. Soc.* **2005**, *127*, 17712. (b) Neumann, R.; Kahan, M. *J. Am. Chem. Soc.* **1998**, *120*, 11969. (c) Neumann, R.; Dahan, M. *Nature* **1997**, *388*, 353. (d) Ben-Daniel, R.; Weiner, L.; Neumann, R. *J. Am. Chem. Soc.* **2002**, *124*, 8788. (e) Hill, C. L.; Brown, R. B., Jr. *J. Am. Chem. Soc.* **1986**, *108*, 536. (f) de Visser, S. P.; Kumar, D.; Neumann, R.; Shaik, S. *Angew. Chem., Int. Ed.* **2004**, *43*, 5661.

(9) (a) Hill, C. L.; Posser-McCartha, C. M. *Coord. Chem. Rev.* **1995**, *143*, 407. (b) Mizuno, N.; Nisono, M. *Chem. Rev.* **1998**, *98*, 199.

(10) (a) Kwen, H.; Tomlinson, S.; Maatta, E. A.; Dablemount, C.; Thouvenot, R.; Proust, A.; Gouzerh, P. *Chem. Commun.* **2002**, 2970. (b) Dablemont, C.; Hamaker, C. G.; Thouvenot, R.; Sojka, Z.; Che, M.; Maatta, E. A.; Proust, A. *Chem. Eur. J.* **2006**, *12*, 9150. (c) Lahootun, V.; Besson, C.; Villanneau, R.; Villain, F.; Chamoreau, L. M.; Boubekeur, K.; Blanchard, S.; Thouvenot, R.; Proust, A. *J. Am. Chem. Soc.* **2007**, *129*, 7127. (d) Proust, A.; Thouvenot, R.; Gouzerh, P. *Chem. Commun.* **2008**, 1837.

(11) Hu, S. Z.; Zhou, Z. H.; Tsai, K. R. *Wuli Huaxue Xuebao* **2003**, *19*, 1073.

(12) (a) Greene, S. N.; Richards, G. J. *Inorg. Chem.* **2004**, *43*, 7030. (b) Serres, R. G.; Grapperhaus, C. A.; Bothe, E.; Bill, E.; Weyhermuller, T.; Neese, F.; Wieghardt, K. *J. Am. Chem. Soc.* **2004**, *126*, 5138.

(13) (a) Decker, A.; Rohde, J. U.; Que, L., Jr.; Solomon, E. I. *J. Am. Chem. Soc.* **2004**, *126*, 5378. (b) Decker, A.; Chow, M. S.; Kemsiey, J. N.; Lehnert, N.; Solomon, E. I. *J. Am. Chem. Soc.* **2006**, *128*, 4719.

(14) (a) Becke, A. D. *Phys. Rev. A* **1988**, *38*, 3098–3100. (b) Perdew, J. P. *Phys. Rev. B* **1986**, *33*, 8822.

(15) Vosko, S. H.; Wilk, L.; Nusair, M. *Can. J. Phys.* **1980**, *58*, 1200.

(16) (a) Te Velde, G.; Bickelhaupt, F. M.; Baerends, E. J.; Fonseca Guerra, C.; van Gisbergen, S. J. A.; Snijders, J. G.; Ziegler, T. *J. Comput. Chem.* **2001**, *22*, 931 (Chemistry with ADF). (b) Fonseca Guerra, C.; Snijders, J. G.; Te Velde, G.; Baerends, E. J. *Theor. Chem. Acc.* **1998**, *99*, 391. (c) *ADF2006. 01, SCM, Theoretical Chemistry*; Vrije Universiteit: Amsterdam, The Netherlands, http://www.scm.com.

(17) (a) Chang, C.; Pelissier, M.; Durand, M. *Phys. Scr.* **1986**, *34*, 394. (b) van Lenthe, E.; Baerends, E. J.; Snijders, J. G. *J. Chem. Phys.* **1993**, *99*, 4597. (c) van Lenthe, E.; Baerends, E. J.; Snijders, J. G. *J. Chem. Phys.* **1994**, *101*, 9783. (d) van Lenthe, E.; van Leeuwen, R.; Baerends, E. J.; Snijders, J. G. *Int. J. Quantum Chem.* **1996**, *38*, 2686.

(18) (a) Klamt, A.; Schü ü rmann, G. *J. Chem. Soc., Perkin Trans.* **1993**, *2*, 799. (b) Klamt, A. *J. Chem. Phys.* **1995**, *99*, 2224. (c) Klamt, A.; Jones, V. *J. Chem. Phys.* **1996**, *105*, 9972. (d) Pye, C. C.; Ziegler, T. *Theor. Chem. Acc.* **1999**, *101*, 396. (e) Pascualahuir, J. L.; Silla, E.; Tunon, I. *J. Comput. Chem.* **1994**, *15*, 1127.

Table 1. Comparison of Experimental and Computational Gas Parameters for Anions 1, 2, and 3

	^{1}**1**		^{1}**2**			^{2}**3**
bond	comp(BP86)	expt	comp(BP86)	comp(PW91)	comp(PBE)	comp(BP86)
r(M−N)	1.640	1.670	1.660	1.661	1.659	1.680
r(M−O_{eq})	2.000	1.970	1.992	1.991	1.992	1.982
r(M−O_{ax})	2.474	2.530	2.484	2.484	2.483	2.532

are 1.41, 1.40, 1.92, 2.10, 2.07, 2.16, and 2.17 Å for N, O, P, W, Ru, Os, and Re, respectively.[19] Spin-unrestricted calculations were performed for all of the open-shell systems in this work.

Single-point calculations were then calculated for the anions at their optimized geometries with B3LYP[20] as implemented in Gaussian 03;[21] the SDD basis set[22] for W and Ru and the 6-31g(d) basis set for all main-group elements were applied in this work. The chemical bonding between the Ru and N atoms in each anion at their ADF-optimized ground-state geometries was evaluated by NBO analysis of the density matrix obtained from B3LYP single-point calculations. All NBO studies were carried out with the NBO 5.0 software package.[23]

3. Results and Discussion

3.1. Ground-State Structures. Earlier calculations on POM species of the Keggin structure showed marginal differences between the X-ray-measured and DFT-optimized geometry. In the present paper, X-ray structures of these monosubstituted Keggin anions are still lacking due to positional disorder.[10c] Thus, by adopting the strategy provided by Neumann et al.[8f] we started from $[PW_{12}O_{40}]^{3-}$ and generated $[PW_{11}O_{39}\{M^{VI}N\}]^{4-}$ (M = Ru, Os, Re) using replacement of a single [W═O] group with [M−N] (M = Ru, Os, Re). The ground state of anions **1** and **2** was found to be the closed-shell singlet state ^{1}**1** and ^{1}**2**, respectively, which fully agrees with the diamagnetic feature of $[PW_{11}O_{39}\{Ru^{VI}N\}]^{4-}$ with C_s symmetry as obtained by experimental measurement.[10c] For the anion **3**, the ground state is the open-shell doublet state ^{2}**3**.[24] For spin-unrestricted calculations, the calculated square of total spin is quite close to its eigenvalues $s(s+1)$, which indicates that spin contamination is minor (see Table S3, Supporting Information).

A comparison of the ground-state (gas-state) parameters shows good agreement between the experimental and the calculated parameters. The computed Ru−N bond length of anion **1**, r(Ru−N) = 1.64 Å, is very similar to the extended X-ray absorption fine structural (EXAFS) values (1.67 Å) (see Table 1).[10c] The calculated average length of four Ru−O bonds (equatorial site) is 2.00 Å; the Ru−O5 distance, with a tetrahedral PO_4^{3-} unit, is 2.47 Å; the largest discrepancy is the Ru−O5 distance where the computed value is 0.06 Å shorter than the experimental value. In many respects, the DFT-optimized and experimental structures for POM systems were similar, as judged by comparison of bond lengths and bond angles; the discrepancy in the bond lengths deviations between theory and experiment was always smaller than 0.1 Å.[25] Although an experimental value of anion **2** is lacking, the Os−N bond lengths calculated by BP86, PW91, and PBE functionals are very similar to each other, r(Os−N) = 1.659−1.661 Å, and in agreement with the reported Os−N distances ranging from 1.525 to 1.703 Å determined by X-ray crystallography.[6b] The M−N distance decreases as M = Re(1.68 Å) > Os(1.66 Å) > Ru(1.64 Å), which can relate this trend to the size of the M atom.

Release of the nitrogen atom is due to cleavage of the M−N bond; as mentioned above, the computed ruthenium−nitrogen bond length is 1.64 Å and displays the triple-bond feature. This bond length in POM was slightly longer than those of nitrido ruthenium complexes with tri- or tetradentate nonporphyrin ligands (1.594−1.615 Å).[26] For visualizing the M−N (M = Ru, Os, Re) binding, we listed some relevant orbitals of anions **1**, **2**, and **3** in Figure 2. It can be found that anions **1**, **2**, and **3** qualitatively have the same bonding scheme. Figure 2 gives a pictorial description of one σ-bonding orbital and two π-bonding orbitals for three anions. The σ-bonding orbitals of anions **1**, **2**, and **3** display the large nitrogen s-orbital character (>80% according to DFT calculations).

The question we are now concerned with is the similarities and differences of the orbital properties of **1**, **2**, and **3** in the ground states, focusing especially on the M−N antibonding interaction. The frontier molecular orbital (FMO) energy level diagrams and relevant molecular orbitals of anions ^{1}**1** and ^{1}**2** are shown in Figure 3, while Table 2 summarizes the electronic structural parameters.

Ruthenium and osmium atoms are in the same group and a different row in the periodic table. This difference generates

(19) Hu, S. Z.; Zhou, Z. H.; Tsai, K. R. *Wuli Huaxue Xuebao* **2003**, *19*, 1073.
(20) (a) Becke, A. D. *Phys. Rev.* **1993**, *98*, 5648. (b) Stephens, P. J.; Devlin, F. J.; Chabalowski, C. F.; Frishch, M. J. *J. Phys. Chem.* **1994**, *98*, 11623.
(21) Frisch, M. J.; Trucks, G. W.; Schlegel, H. B.; Scuseria, G. E.; Robb, M. A.; Cheeseman, J. R.; Montgomery, J. A., Jr.; Vreven, T.; Kudin, K. N.; Burant, J. C.; Millam, J. M.; Iyengar, S. S.; Tomasi, J.; Barone, V.; Mennucci, B.; Cossi, M.; Scalmani, G.; Rega, N.; Petersson, G. A.; Nakatsuji, H.; Hada, M.; Ehara, M.; Toyota, K.; Fukuda, R.; Hasegawa, J.; Ishida, M.; Nakajima, T.; Honda, Y.; Kitao, O.; Nakai, H.; Klene, M.; Li, X.; Knox, J. E.; Hratchian, H. P.; Cross, J. B.; Bakken, V.; Adamo, C.; Jaramillo, J.; Gomperts, R.; Stratmann, R. E.; Yazyev, O.; Austin, A. J.; Cammi, R.; Pomelli, C.; Ochterski, J. W.; Ayala, P. Y.; Morokuma, K.; Voth, G. A.; Salvador, P.; Dannenberg, J. J.; Zakrzewski, V. G.; Dapprich, S.; Daniels, A. D.; Strain, M. C.; Farkas, O.; Malick, D. K.; Rabuck, A. D.; Raghavachari, K.; Foresman, J. B.; Ortiz, J. V.; Cui, Q.; Baboul, A. G.; Clifford, S.; Cioslowski, J.; Stefanov, B. B.; Liu, G.; Liashenko, A.; Piskorz, P.; Komaromi, I.; Martin, R. L.; Fox, D. J.; Keith, T.; AlLaham, M. A.; Peng, C. Y.; Nanayakkara, A.; Challacombe, M.; Gill, P. M. W.; Johnson, B.; Chen, W.; Wong, M. W.; Gonzalez, C.; Pople, J. A. *Gaussian 03, revision C.02*; Gaussian, Inc.: Wallingford, CT, 2004.
(22) Dunning, T. H., Jr.; Hay, P. J. *Modern Theoretical Chemistry*. Schaefer H. F., III, Ed.; Plenum: New York, 1976; Vol. *3*, pp 1−28.
(23) Glendening, E. D.; Badenboop, J. K.; Reed, A. E.; Carpenter, J. E.; Bohmann, J. A.; Morales, C. M.; Weinhold, F. *NBO 5.0*; Theoretical Chemistry Institute, University of Wisconsin: Madison, WI, 2001.
(24) Guan, W.; Yang, G. C.; Liu, C. G.; Song, P.; Fang, L.; Yan, L. K.; Su, Z. M. *Inorg. Chem.* **2008**, *47*, 5245.
(25) Maestre, J. M.; Lopez, X.; Bo, C.; Poblet, J.-M.; Casan-Pastor, N. *J. Am. Chem. Soc.* **2001**, *123*, 3749.
(26) Leung, S. K. Y.; Huang, J. S.; Liang, J. L.; Che, C. M.; Zhou, Z. Y. *Angew. Chem., Int. Ed.* **2003**, *42*, 340.

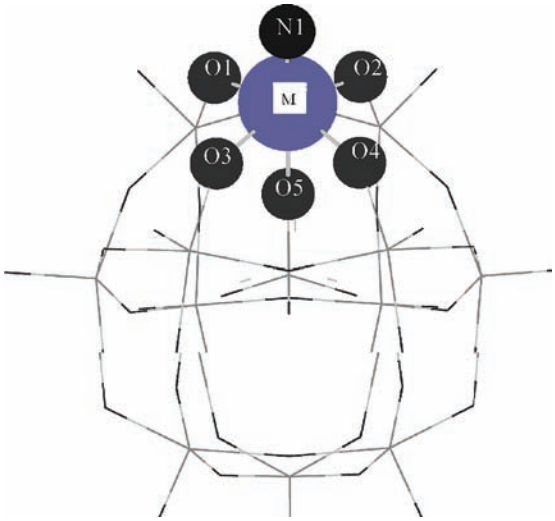

Figure 1. Geometrical structures of $[PW_{11}O_{39}\{M^{VI}N\}]^{4-}$ (**1**, M = Ru; **2**, M = Os; **3**, M = Re). The most important bond lengths are given in Table 1 (where O5 denoted the oxygen of the tetrahedral PO_4^{3-} unit).

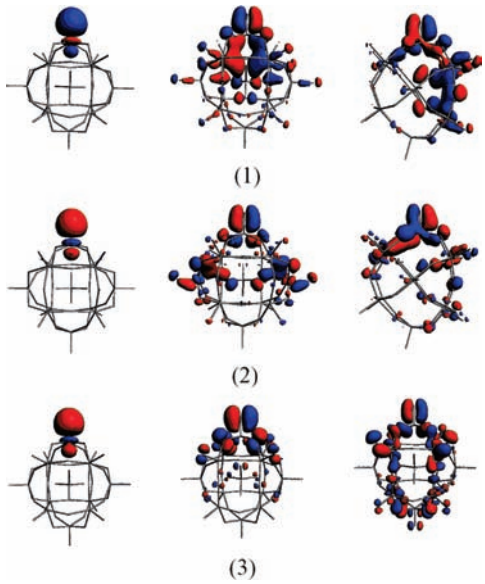

Figure 2. Plot of some relevant orbitals of anions **1**, **2**, and **3** showing visualization of the M−N (M = Ru, Os, Re) bonding.

the different d-orbital splitting. The whole FMO energies of anion **2** are shifted to higher energies relative to anion **1**; the energy of the nonbonding orbital (HOMO) is shifted by ∼0.5 eV. On the other hand, the LUMO and LUMO+1 of anion **1**, two nearly degenerate unoccupied orbitals, are Ru−N antibonding orbitals with π symmetry. This result fits the widely accepted Ballhausen and Gray d-orbital splitting pattern for pseudo-octahedral complexes with one multiply bonded ligand.[27] However, in anion **2**, the strong Os−N antibonding orbitals are shifted to the higher unoccupied orbitals (LUMO+4, LUMO+5) (see Figure 3); LUMO and LUMO+1 of anion **2** are mainly formed by the contributions of the tungsten d orbitals, which are not related to the Os−N bond. Although LUMO+2 and LUMO+3 have contributions from the OsN unit, the low compositions determine that the two orbitals are not strong Os−N antibonding orbitals. Unfortunately, for anion **3**, we did not find the Re−N antibonding orbitals in the 10 lowest unoccupied orbitals (see Table 2).

In anion **1**, the contributions of the RuN unit in LUMO and LUMO+1 are ∼83% and ∼78%, respectively. It is larger than that of the OsN unit in LUMO+4 and LUMO+5 (73% and 47%) for anion **2**. The larger RuN unit compositions of **1** compared to **2** mainly arise from the compositions of the nitrogen p orbital. All of the results indicate that anion **1** possesses a stronger antibonding interaction between the metal and the nitrogen atoms than that of anions **2** and **3**.

According to the FMO theory, a good electrophile requires low-lying unoccupied orbitals with high molecular orbital compositions on the reacting atom to achieve good overlap with the FMOs on the nucleophilic reagent (such as triphenylphosphine).[1b,15,28] In our studied systems, the M−N antibonding orbitals are the key FMOs; the nitrogen atom is the reacting atom, which interacts with the electron density of the nucleophilic reagent. As mentioned above, these differences in the calculated FMOs and especially the antibonding orbitals provide insight into the differences in reactivity between anions **1** and **3**. Obviously, the reactivity of the two anions are significantly different; anion **1** exhibits high reactivity and is capable of bonding the triphenylphosphine. However, anion **3** cannot provide the effective unoccupied orbitals and thus gives disappointing reactivity. All of the results are in agreement with the experimental studies.[10c] We found that anion **1** has stronger and lower-energy Ru−N antibonding orbitals compared with anions **2** and **3**, and thus, anion **1** is a stronger electrophile than **2** and **3** according to our DFT calculations.

On the basis of the strong antibonding interaction in anion **1**, the substitution effects of the central tetrahedron heteroatoms (XO_4, X = Al, Si, P, As) have been considered; the optimized key geometrical parameters are presented in Table 3. The results show that the Ru−N bond length decreases in the order Al(III) > Si(IV) > P(V) > As(V); the calculated values, r(Ru−N) = 1.639−1.655 Å, are very similar. The bond lengths in Table 3 also show that there are not significant changes with replacement of the tetrahedron heteroatoms.

The relative energy of the LUMO increases in the order Al(III) < Si(IV) < P(V) ≈ As(V) (see Figure 4). Obviously, the anion charge significantly affects the orbital energies. The relative energy of the LUMO in $[PW_{11}O_{39}\{Ru^{VI}N\}]^{4-}$ is 0.22 eV larger than that of $[AlW_{11}O_{39}\{Ru^{VI}N\}]^{6-}$. However, the order and composition of the RuN antibonding orbitals (LUMO and LUMO+1) in each anion does not change with replacement of the central tetrahedron heteroatoms. According to the orbital diagram in Figure 4, a direct consequence is that the first reductions in these anions take place at the RuN functional group. Simultaneously, the RuN antibonding orbitals (LUMO and LUMO+1) indicate that the extent of the bonding interaction between the Ru and N atoms would be weakened in the reduced process.

(27) Balhausen, C. J.; Gray, H. B. *Inorg. Chem.* **1962**, *1*, 111.

(28) Romo, S.; Antonova, N. S.; Carbo, J. J.; Poblet, J. M. *Dalton Trans.* **2008**, 5166.

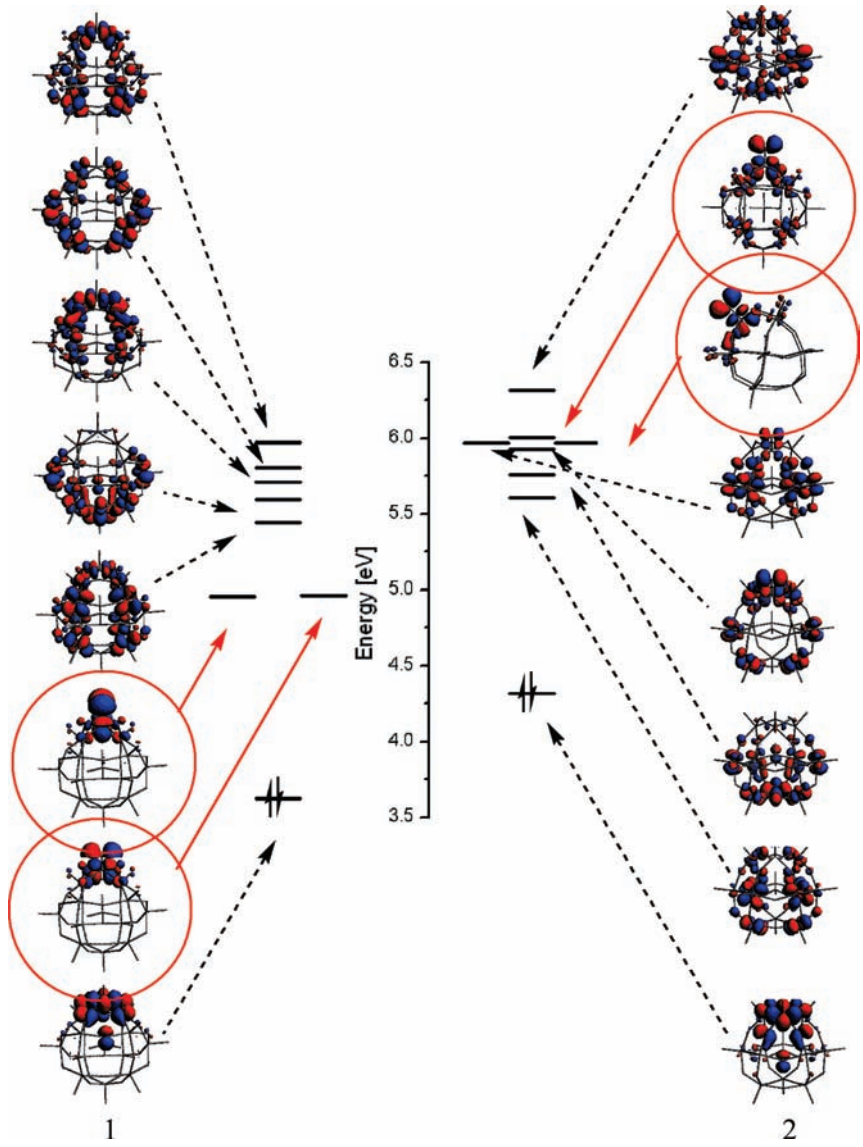

Figure 3. Frontier molecular orbitals for anions ^{1}**1** and ^{1}**2**.

Table 2. Electronic Structure Parameters for Anions 1, 2, and 3

	^{1}**1**			^{1}**2**			^{2}**3**					
	Ru	N	POM	Os	N	POM	Re(α)	Re(β)	N(α)	N(β)	POM(α)	POM(β)
charges	1.89	−0.47	−5.42	2.01	−0.54	−5.48	2.08		−0.61		−5.47	
						MO[%]						
LUMO	37	45	18	0	0	100	0	36	0	0	100	0
LUMO+1	34	44	22	0	0	100	2	0	0	0	98	100
LUMO+2	5	0	95	12	11	77	0	9	0	0	100	91
LUMO+3	0	0	100	5	5	90	0	0	0	0	100	100
LUMO+4	19	0	81	33	40	27	9	0	0	0	91	100
LUMO+5	0	0	100	22	26	52	0	12	0	0	100	88

Table 3. Optimized Geometries of $[XW_{11}O_{39}\{Ru^{VI}N\}]^{n-}$ (X = Al, Si, P, As)

bond	$[AlW_{11}O_{39}\{Ru^{VI}N\}]^{6-}$	$[SiW_{11}O_{39}\{Ru^{VI}N\}]^{5-}$	$[PW_{11}O_{39}\{Ru^{VI}N\}]^{4-}$	$[AsW_{11}O_{39}\{Ru^{VI}N\}]^{4-}$
M−N	1.655	1.649	1.640	1.639
M−O_1	2.038	2.013	2.010	2.023
M−O_2	2.038	2.013	2.010	2.023
M−O_3	1.999	1.986	1.987	1.999
M−O_4	1.999	1.986	1.987	1.999
M−O_5	2.286	2.389	2.474	2.372

3.2. Excited-State Structures of Anions 1 and 2. The orbitals associated with the RuN functional group and their adjacent orbitals of $[PW_{11}O_{39}\{Ru^{VI}N\}]^{4-}$ are shown in Figure 5, where the π*-antibonding interaction between the nitrogen and the ruthenium atoms is mostly across the RuN functional group (π_{xz}*, π_{yz}*). Thus, we calculated a triplet state with a

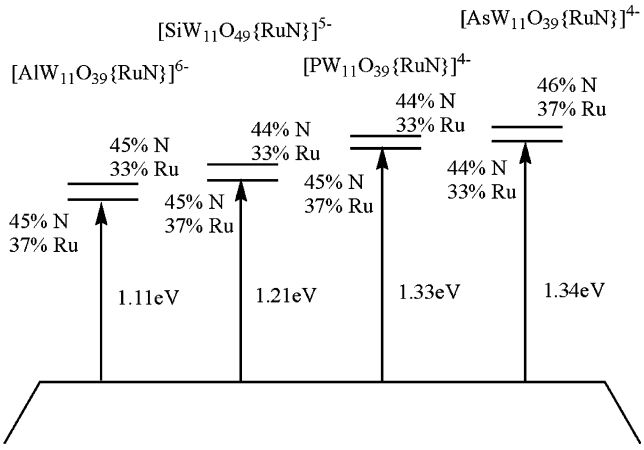

Figure 4. Molecular orbitals scheme for several $[XW_{11}O_{39}\{RuN\}]^{n-}$ (X = Al, Si, P, As) anions.

$\delta^1\pi^1$ configuration and a quintet state with an oxo$^1\delta^1\pi^{*1}\pi^{*1}$ configuration, where the two Ru−N π*-antibonding orbitals are successively occupied in the two spin states. The corresponding triplet and quintet state ^{3}**1** and ^{5}**1** were 24.54 and 61.23 kcal/mol higher than the ground state. The key optimized bond lengths for ^{3,5}**1** are listed in Table 4. This weakening of the Ru−N bond by the electron shifting to Ru−N π*-antibonding orbitals leads to a distortion of the Ru−N bond length in the excited state. The Ru−N bond gets longer as these Ru−N π*-antibonding orbitals are occupied in different spin states; the difference in the Ru−N bond length between the singlet and quintet states is 0.42 Å. In the equatorial plane, the average Ru−O bond length in the excited states is shorter than that of the ground state, which indicates there is more bonding interaction in the equatorial plane in the excited states compared to the ground state.

The spin densities in the two high spin states ^{3}**1** and ^{5}**1** are shown in Table 5; it can be found that the spin densities in ^{3}**1** and ^{5}**1** are localized on the RuN unit (1.5 and 3.3); some spin densities are located on the four coordinated oxygen atoms (O1−O4). This feature is in good agreement with the electronic structures in Figure 3, which demonstrates that the Ru−N π* orbitals have been occupied in two high spin states.

By contrast, we optimized the geometry of the excited state with the electronic configuration ^{3}**2** and ^{5}**2** corresponding to anion **1**; in two excited states of anion **2**, the increase in the Os−N bond lengths is Δr(Os−N) = +0.01 and +0.03 Å for ^{3}**2** and ^{5}**2**, respectively (see Table 4). This increase in the Os−N distance is not significant when compared with the Ru−N bond length in the excited states. This feature results from the LUMO and LUMO+1 of anion **2** not being Os−N antibonding orbitals. The trend of a larger increase in the Ru−N bond length of anion **1** relative to anion **2** in the excited states reflects the more effective order and composition of FMOs.

3.3. Redox Properties. The one-electron-reduced species ^{2,4}**1**$_{\mathbf{reduced}}$, ^{2}**2**$_{\mathbf{reduced}}$, and ^{1}**3**$_{\mathbf{reduced}}$[10c] have been optimized. For anion **1**, the high-spin state ^{4}**1**$_{\mathbf{reduced}}$ is 25.97 kcal/mol higher than that of the doublet state, ^{2}**1**$_{\mathbf{reduced}}$. It is well known that POMs can be reduced by addition of various numbers of electron; the geometrical structures of the reduction products still retain the general structures of their oxidized parents because the additional electrons are delocalized over the nonbonding metal d-like orbitals. However, for anion **1**, LUMO and LUMO+1 are the localized Ru−N antibonding orbitals; thus, the reduced process would significantly alter the Ru−N distance. Table 4 gives key data from theoretical computations on the "gas-phase" structure of one-electron-reduced species in anions **1**, **2**, and **3**. For anion **1**, it can be found that the Ru−O bond length in the equatorial plane and the Ru−O5 bond length do not alter significantly in the one-electron-reduced process. However, the Ru−N bond length gets a larger increase compared with these Ru−O bond lengths in the one-electron-reduced process, Δr(Ru−N) = 0.065 and 0.146 Å for ^{2}**1**$_{\mathbf{reduced}}$ and ^{4}**1**$_{\mathbf{reduced}}$, respectively. By contrast, the M−N (M = Os, Re) bond distances of anions **2** and **3** are almost constant in the reduction process.[24]

As mentioned above, the LUMO of ^{1}**1** is composed of about ~45% N and ~37% Ru; it is more likely that the RuN unit will prefer to accept the electrons when the anion is reduced. However, for anions **2** and **3**, the OsN and ReN units would not be the reduction center according to molecular orbital analysis. Unrestricted calculations of one-electron-reduced species were performed to check predictions made by molecular orbital analysis. The spin polarizations in Table 5 show that the additional electron in ^{2}**1**$_{\mathbf{reduced}}$ localizes on the N center with a 0.57 spin alpha electron and the Ru center with a 0.29 spin alpha electron. In other words, the one-electron-reduced species of anion **1** may be described as having substantial $[PW_{11}O_{39}\{Ru^{VI}N^{\bullet}\}]^{5-}$ character, even though in the high-spin state of reduction species ^{4}**1**$_{\mathbf{reduced}}$, the N atom still carries a large spin density (1.12 of N vs 1.09 of Ru). This feature does not change when solvation is included. For anion **2**, the reduced electron in ^{2}**2**$_{\mathbf{reduced}}$ localizes on the POM ligands; the spin density on the OsN units is very low, which demonstrates that the OsN unit is not the reduced center (see Table 5). We calculated the four-electron-reduced process of anion **3**;[24] the results showed that the reduction center of anion **3** is the rhenium core.

3.4. Bonding Analysis of the Ru−N Bond in the Ground and Excited States. In order to investigate the bonding feature between the Ru and N centers in the present paper, the extent of bonding interaction between the Ru and N centers in the $[PW_{11}O_{39}\{RuN\}]^{4-}$ anion with different spin states was computed using NBO theory. The conventional parameters are frequently used to characterize the bonding situation in molecules; the bond orders and NBO distribution have been analyzed in this work.

The calculated Wiberg bond indices (WBI) in $[PW_{11}O_{39}\{RuN\}]^{4-}$ with different spin states and oxidizing states are listed in Table 6; the results indicate that the Ru−N bond possesses triple-, double-, and single-bond character when moving along the change of spin state (^{1}**1** → ^{3}**1** → ^{5}**1**) (see Figure 6), as supported by (i) the calculated WBI values of 2.374, 1.815, and 0.96 (Table 6), (ii) the three doubly occupied bonding NBOs, four singly occupied, and two singly occupied bonding NBOs between the Ru and N

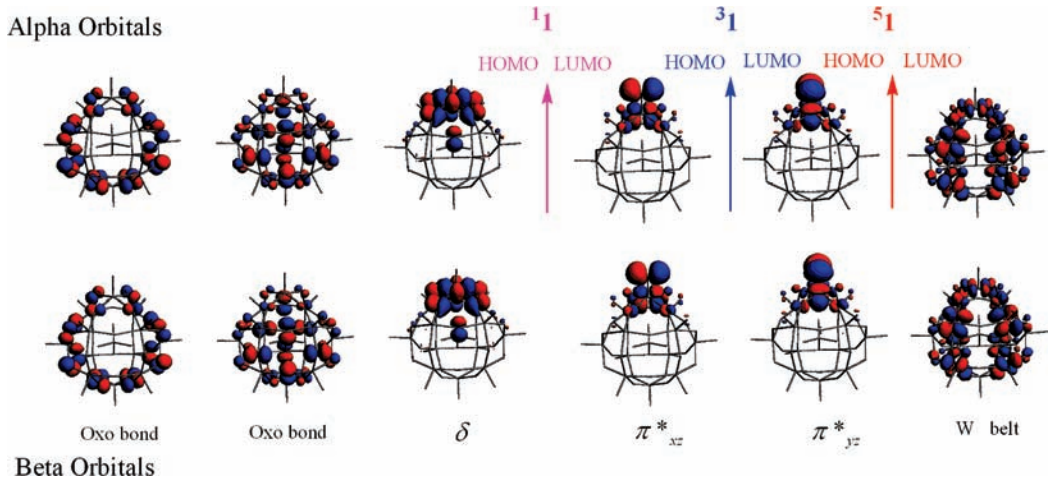

Figure 5. Molecular orbitals of $[PW_{11}O_{39}\{Ru^{VI}N\}]^{4-}$.

Table 4. Comparison of Calculated M−X (M = Ru, Os; X = N, O) Bond Length in the Ground States, Excited States, and One-Electron-Reduced Species for Anions 1, 2, and 3

bond	^{1}**1**	^{3}**1**	^{5}**1**	^{2}**1**$_{reduced}$	^{4}**1**$_{reduced}$	^{1}**2**	^{3}**2**	^{5}**2**	^{2}**2**$_{reduced}$	^{2}**3**	^{1}**3**$_{reduced}$
M−N	1.640	1.723	1.957	1.705	1.786	1.660	1.671	1.691	1.666	1.680	1.681
M−O_1	2.010	2.008	1.993	2.082	2.027	2.003	1.958	1.972	2.004	1.983	2.009
M−O_2	2.010	1.996	1.976	2.024	2.031	2.003	1.964	1.973	2.004	1.983	2.009
M−O_3	1.987	1.984	1.966	1.991	1.997	1.981	1.935	1.948	1.976	1.982	1.994
M−O_4	1.987	1.997	1.986	2.044	2.024	1.981	1.938	1.948	1.976	1.982	1.994
M−O_5	2.474	2.392	2.330	2.463	2.390	2.484	2.453	2.463	2.498	2.532	2.558

Table 5. Mulliken Charge and Spin Density of Selected Atoms in Anions 1, 2, and 3

	^{1}**1**		^{3}**1**		^{5}**1**	
atom	Mulliken	spin	Mulliken	spin	Mulliken	spin
M	1.894		1.820	0.924	1.773	1.527
N	−0.470		−0.491	0.611	−0.479	1.760
O1	−0.885		−0.868	0.090	−0.872	0.094
O2	−0.945		−0.880	0.072	−0.875	0.135
O3	−0.904		−0.903	0.066	−0.889	1.527
O4	−0.904		−0.892	0.084	−0.888	1.760
O5	−1.021		−1.020	−0.001	−1.018	0.094

	^{2}**1**$_{reduced}$		^{4}**1**$_{reduced}$		^{1}**2**	
atom	Mulliken	spin	Mulliken	spin	Mulliken	spin
M	1.527	1.689	0.289	1.679	2.015	
N	1.760	−0.575	0.573	−0.584	−0.537	
O1	0.094	−0.867	0.018	−0.875	−0.902	
O2	0.135	−0.890	−0.009	−0.877	−0.902	
O3	1.527	−0.908	−0.012	−0.897	−0.926	
O4	1.760	−0.883	0.007	−0.887	−0.926	
O5	0.094	−1.011	−0.002	−1.009	−1.025	

	^{2}**2**$_{reduced}$		^{2}**3**		^{1}**3**$_{reduced}$	
atom	Mulliken	spin	Mulliken	spin	Mulliken	spin
M	2.0135	0.005	2.082	0.670	1.960	
N	−0.593	0.002	−0.610	−0.086	−0.674	
O1	−0.914	0.016	−0.922	0.024	−0.919	
O2	−0.914	0.016	−0.922	0.024	−0.919	
O3	−0.932	0.012	−0.938	0.015	−0.928	
O4	−0.932	0.012	−0.938	0.015	−0.928	
O5	−1.023	−0.001	−1.022	−0.000	−1.018	

centers in singlet, triplet, and quintet spin states, respectively (see Table S1, Supporting Information), and (iii) the Ru−N bond gets longer from 1.64 to 1.96 Å with the change of spin state. Inspection of natural hybrid orbital (NHO) compositions and occupancies suggests that the bonding interactions between the Ru and N centers are σ and π symmetry for ^{1,3}**1** and σ symmetry for ^{5}**1** (Table S1, Supporting Information). In all the NHO, the polarization coefficients between the Ru and N centers are not significantly different, which suggests the covalent character of the Ru−N bonds. NBO analysis of ^{2}**1**$_{reduced}$ suggests that the bonding interaction between the Ru and N centers is very similar in terms of symmetry and bond order to the calculations for ^{3}**1** (see Table 1). The Ru−N bond in ^{2}**1**$_{reduced}$ has obvious double-bond nature, as indicated by the calculated bond order of 1.967. For the singlet state of anion ^{1}**1**, the ruthenium(VI) core processes a $4d^2$ configuration; NBO calculations indicated that one lone pair (lp) on the ruthenium atom has mainly d character and is practically occupied by two electrons, which indicates this 4d orbital of the ruthenium atom was not the bonding atomic orbital. It agrees with the DFT calculations, that is, the nonbonding double-occupied δ d-metal orbital (HOMO) in ^{1}**1** (see Figures 3 and 5). All

Table 6. Selected NBO-Calculated Wiberg Bond Indices (WBI) in Anion 1

bond	^{1}**1**	^{3}**1**	^{5}**1**	^{2}**1**$_{reduced}$	^{4}**1**$_{reduced}$
Ru−N	2.374	1.815	0.960	1.967	1.262
Ru−O_1	0.474	0.481	0.479	0.392	0.433
Ru−O_2	0.474	0.5001	0.537	0.391	0.424
Ru−O_3	0.470	0.4791	0.532	0.395	0.430
Ru−O_4	0.470	0.455	0.458	0.399	0.407
Ru−O_5	0.078	0.090	0.108	0.075	0.078

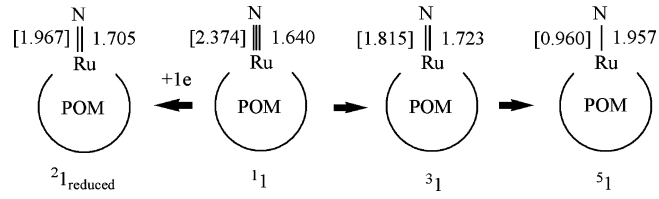

Figure 6. Bonding interactions between Ru and N centers according to the NBO Analysis (values are bond lengths and bond orders (in brackets) of the Ru−N bond).

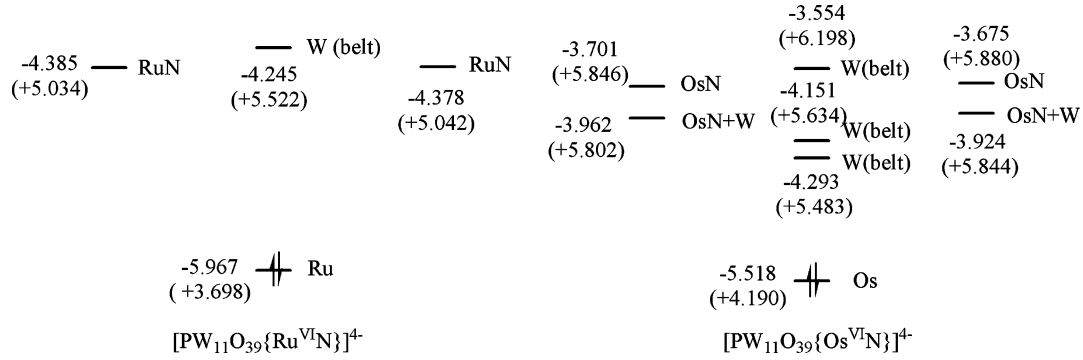

Figure 7. Molecular orbital scheme for anions **1** and **2** in acetonitrile and the gas phase (in parentheses).

of the results reveal that the bonding interaction between the ruthenium and nitrogen atoms can be weakened by modification of the spin and oxidation stats, which is summarized in Figure 6.

3.5. Solvent Effects. As mentioned above, the order and composition of FMOs of these anions is an important factor in determination of their reactivity, redox properties, and excited-state structures. However, it is well known that highly charged anions do not exist in the gas phase; moreover, FMOs of the negatively charged system are sensitive to the size of the basis sets. Thus, single-point calculations with their ADF-optimized ground-state geometries in the gas phase, continuum solvation model COSMO, a dielectric constant of acetonitrile, and a large size basis sets in ADF program, TZ2P, which is core double-ζ, valence triple-ζ, doubly polarized basis, have been employed for solvent and basis considerations. Figure 7 gives the energy of some FMOs for anions **1** and **2** in acetonitrile solution and in the gas-phase (in parentheses); it is found that the solvation effect significantly decreases the FMO energies. For anion **1**, the LUMO and LUMO+1 appear at quite negative energies (about −4.38 eV). The FMO energies of anions **2** and **3** also give the same feature. However, the relative energies between these FMOs did not change largely when compared with the absolute FMO energies; the HOMO−LUMO gap for anion **2** in the gas phase is 1.2 eV and in solution 1.3 eV. In addition, we did not observe any distinct difference in the order and composition of FMOs of anions **1**, **2**, and **3** between the gas phase and solution provided by solvent calculations with large size basis sets (see Figure 7). Therefore, the study of the electronic structure of the gas-phase anion is enough to understand the reactivity, redox properties, and excited-state structures of these POMs.

4. Summary

In this paper, we describe systematic DFT calculations for ground states, excited states, and reduction states of Keggin-type POMs, $[PW_{11}O_{39}\{MN\}]^{4-}$ (M = Ru, Os, Re). The results show that anion **1** possesses strong antibonding interactions between the metal and nitrogen atoms. A large increase in the Ru−N bond length of anion **1** in the excited states has been found; the effective order and composition of FMOs in anion **1** is the key factor. For anion **1**, the substitution effects of the central tetrahedron heteroatoms (XO_4, X = Al, Si, P, As) affect the relative energy of LUMO; the relevant orbital energies increase in the order Al(III) < Si(IV) < P(V) ≈ As(V). The order and composition of FMOs and the geometrical structures are almost independent of the nature of X. The RuN unit in anion **1** is the reduced center, and the Ru−N bond length increases in the one-electron-reduced process, but the lengths of the Os−N and Re−N bonds for anions **2** and **3** are not significantly changed in the reduced processes. NBO analysis of the extent of bonding interaction between the ruthenium and nitrogen centers in anion **1** shows that the Ru−N bond possesses a covalent feature and displays triple-, double-, and single-bond character when moving along the change of spin state (^{1}**1** → ^{3}**1** → ^{5}**1**).

Acknowledgment. The authors gratefully acknowledge the financial support from the National Natural Science Foundation of China (Project Nos. 20373009 and 20703008), Chang Jiang Scholars Program (2006), Program for Changjiang Scholars and Innovative Research Team in University (IRT0714), the National High-tech Research and Development Program (863 Program 2007AA03Z354), the Science Foundation for Young Teachers of NENU (20070304 and 20070309), and the Training Fund of NENU's Scientific Innovation Project (NENU-STC07017). We also thank Yuhe Kan for computational support.

Supporting Information Available: The NHO composition of $[PW_{11}O_{39}\{Ru^{VI}N\}]^{4-}$ in different spin states and reduced states, the occupation and hybridization of lone pairs of Ru and N atoms in $[PW_{11}O_{39}\{Ru^{VI}N\}]^{4-}$ with different spin states and reduced states, and exact and expectation value of the total spin for all open-shell systems. This material is available free of charge via the Internet at http://pubs.acs.org.

IC8012443